Available online at www.sciencedirect.com
SCIENCE DIRECT®
International Journal of Heat and Fluid Flow 27 (2006) 566–575
International Journal of HEAT AND FLUID FLOW
www.elsevier.com/locate/ijhff

Reynolds number scaling in a non-equilibrium turbulent boundary layer with mild adverse pressure gradient

Carolyn D. Aubertine, John K. Eaton *

Department of Mechanical Engineering, Stanford University Stanford, CA 94305-3030, USA

Available online 31 March 2006

Abstract

High resolution laser Doppler anemometer measurements were acquired in a two-dimensional turbulent boundary layer over a four degree ramp at three momentum thickness Reynolds numbers: 3300, 14,100 and 20,600. The goal was to examine an adverse pressure gradient boundary layer far from separation in order to develop turbulent stress scalings to collapse the adverse pressure gradient and flat plate stress profiles over a range of Reynolds numbers. The flow develops as a flat plate boundary layer before being subjected to a varying pressure gradient along the length of a four degree straight ramp. Mean velocity measurements show a log law region for all velocity profiles. The stresses however are perturbed by the pressure gradient with the streamwise normal stress developing an extended outer layer plateau and the wall-normal stress displaying a growing outer layer peak. Scaling parameters are proposed to collapse the inner and outer layer regions of the normal stresses for both the adverse pressure gradient and flat plate profiles over the range of Reynolds numbers examined.

Keywords: Turbulence; Boundary layer; Pressure gradient; Reynolds-number scaling

1. Introduction

Adverse pressure gradient boundary layers occur in many practical applications, for example diffusers and the aft section of ship hulls, and they often play critical roles in the performance of these devices. The study of adverse pressure gradients has been carried out in a wide variety of flows and a discussion of some of the work in this area can be found in Aubertine and Eaton (2005). While there has been wide interest in these flows, little work has been performed to determine scalings capable of collapsing the mean and turbulent velocity profiles over varying conditions.

The scaling of the mean flow and the turbulent stresses has been previously examined in a variety of different flows. For the flat plate boundary layer, the effects of Reynolds number were found by DeGraaff and Eaton (2000) to disappear using a new mixed scaling determined empirically from a flat plate data set taken over a moderate Reynolds number range. This scaling collapses the wall normal stress and the Reynolds shear stress using the standard normalization of $\overline{v'^2}/u_\tau^2$ and $\overline{u'v'}/u_\tau^2$ respectively, where u_τ is the friction velocity defined as $\sqrt{\tau_{\text{wall}}/\rho}$. However, the streamwise normal stress collapse was shown to occur using the mixed scaling $\overline{u'^2}/u_\tau U_e$, where U_e is the local freestream velocity. This scaling cannot be supported using classical arguments; however, recent work by Marusic and Kunkel (2003) has helped to explain why this scaling holds. To extend the Reynolds number range for which this scaling has been tested, Metzger et al. (2001) re-examined the results of Klewicki and Falco (1990), showing that this new scaling also held for experiments run at Reynolds numbers up to $Re_\theta = 5{,}000{,}000$. Re_θ is the Reynolds number based on momentum thickness, θ.

Elsberry et al. (2000) examined an equilibrium boundary layer near separation. The flow for this study was highly anisotropic and while the mean flow was in equilibrium, the turbulence was not found to be in equilibrium with the mean flow. When the turbulent stresses were scaled on the freestream velocity an increase in the scaled stress values was observed as the flow traveled farther downstream. The mean velocity in the flow was found to be

* Corresponding author. Tel.: +1 650 723 1971; fax: +1 650 725 4862.
E-mail addresses: caubertine@stanfordalumni.org (C.D. Aubertine), eaton@vk.stanford.edu (J.K. Eaton).

0142-727X/$ - see front matter © 2006 Elsevier Inc. All rights reserved.
doi:10.1016/j.ijheatfluidflow.2006.02.004

approximately self-similar and this was then used to determine similarity scales which lead to scalings to collapse the various stresses. They determined a scaling to collapse the correlation coefficient, $\frac{\overline{u'v'}}{\sqrt{\overline{u'^2}\overline{v'^2}}}\frac{U_e}{U_o}$. Here U_o is defined as the maximum value of the freestream velocity found over the entire flow field. To collapse the location of the peak in the correlation coefficient, a new length scale was empirically determined, $\frac{y}{\theta Re_\theta^{0.2}}$. The turbulent stresses were then found to collapse using the same length scale and either U_o^2 for the streamwise and wall normal stresses, or $U_o U_e$ for the Reynolds shear stress. Since the similarity scales for the mean flow and turbulence are not the same, the flow is not in equilibrium and the scales used to collapse the turbulent stresses are most likely not unique.

The mean velocity profile has been examined by a number of groups with the goal of collapsing the profiles in different regions of the boundary layer. The logarithmic law of the wall has been observed to hold in a wide variety of adverse pressure gradient boundary layers; however, the growing wake associated with these boundary layers leads to changing profile shapes, particularly in the outer layer. It is these profile changes that a number of groups have attempted to develop scalings to collapse. Bernard et al. (2003) examined the flow over a half airfoil. The mean flow in the inner region faithfully followed the logarithmic law of the wall, while the wake strength changed as the flow progressed. They determined a new length scale which allowed them to collapse the linear inner wake onto a profile that appears to tend toward a universal profile. Using DNS for a strong adverse pressure gradient, Skote and Henningson (2002) found that far from the wall the mean velocity profiles could be collapsed using a pressure gradient velocity scale of $u_p = (\frac{\nu}{\rho}\frac{dP}{dx})^{1/3}$. A mean velocity defect law proposed by Mellor and Gibson (1966) used a pressure velocity of $u_p = \sqrt{\frac{\delta^*}{\rho}\frac{dP}{dx}}$ as the velocity scale for the outer layer, where δ^* is the displacement thickness.

Reynolds number scaling in more complicated flows has also been examined. In the separating and reattaching boundary layer flow of Song and Eaton (2004), the scaling of the turbulent stresses at the separation point, a location of strong adverse pressure gradient with curvature was examined. The length scale necessary to collapse the peaks for both the normal stresses and the shear stress was found to be $y/y_{\text{inflection}}$, where $y_{\text{inflection}}$ is the location of the inflection point in the mean flow. For the streamwise normal stress the stress scaled on the empirically determined $U^2_{\text{inflection}}$, where $U_{\text{inflection}}$ is the velocity of the mean flow at the inflection point. The wall normal stress was found to scale on the value of $u^2_{\tau,\text{ref}}$, the value of the friction velocity in the boundary layer prior to the start of the adverse pressure gradient. These velocity scales are much more complicated than those of the flat plate boundary layer and could be dependent on the particular flow geometry; however, these scalings show that for a strong adverse pressure gradient, the stresses do not scale on the same parameters that are important for a flat plate boundary layer.

In more complex boundary layer flows such as those of DeGraaff and Eaton (1999) and Song and Eaton (2004), which were subjected to strong pressure gradients, separation, reattachment and curvature, the flat plate boundary layer scaling of DeGraaff and Eaton (2000) was observed to hold near the wall as soon as the pressure gradients were removed. In these flows, as the boundary layer relaxed back toward equilibrium on a flat plate a stress equilibrium layer began to form in the flow adjacent to the wall as soon as the pressure gradient dropped to zero. In this growing stress equilibrium layer, the normalized stress profiles were identical to those in a flat plate and the mixed scaling of DeGraaff and Eaton (2000) held. From a computational modeling perspective, this is an important result as wall functions can be comfortably used in these flows. Unfortunately, this scaling appears to only hold in zero pressure gradient flows and as soon as the flow is subjected to even a mild pressure gradient no scaling has been found to collapse the turbulence stress data onto a simple profile, such as that of the flat plate boundary layer. A similar near-wall scaling valid in non-equilibrium pressure gradient flows would be very useful.

The objective of the current experiment is to examine a relatively mild adverse pressure gradient produced by a slow linear expansion of the test section. The pressure gradient was large enough to perturb the boundary layer from its flat plate state, but small enough to avoid separation. Stress measurements along the length of this extended region of pressure gradient can help to identify the existence of a universal scaling for such boundary layers. This paper describes the effect of changing the Reynolds number on the flow development and proposes new scalings valid for collapsing the adverse pressure gradient profiles, as well as examining previously proposed scalings to collapse the mean velocity and turbulence profiles for a moderate range of Reynolds numbers.

2. Experiments

The experiments were performed in a closed loop wind tunnel, which is mounted inside a pressure vessel. The measurements were made with a two component, high-resolution laser Doppler anemometer (LDA) described by DeGraaff and Eaton (2001). The wind tunnel test section has a rectangular cross section and is 152 mm by 711 mm by 2.9 m in length. The boundary layer is tripped 150 mm downstream of a 5:1 contraction and develops over a 1.5 m long flat plate. The flow is then mildly contracted over a streamwise distance of 169 mm on the bottom wall, reducing the test section height from 152 mm to 131 mm. The boundary layer then relaxes to equilibrium characteristics on a 480 mm long flat plate. At a typical freestream velocity of 15 m/s, the freestream turbulence level is approximately 0.2%.

The flow geometry (Fig. 1) consists of part of the 480 mm flat plate and a 4° linear expansion. The ramp expands the tunnel height from 131 mm to 152 mm. The

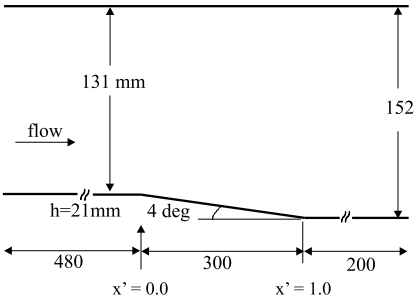

Fig. 1. Current flow geometry.

ramp height, h is equal to the amount the tunnel height expands, 21 mm. The flow does not separate along this ramp. The trailing edge of the ramp produced a small step in height between the ramp surface and the bottom surface of the wind tunnel. This step was patched using spackling and was sanded smooth. Due to this non-ideal flow surface at the trailing edge of the ramp, the flow is perturbed by surface curvature, which is not well defined. The data gathered at this location are not included owing to this non-ideal surface.

The custom LDA has a measurement volume 35 μm in diameter and 60 μm in length. Normalized using inner units, the measurement volume ranges in diameter from 1.8 to 9.8 over the range of Reynolds numbers examined here. Due to its small measurement volume, two of the major uncertainty sources – velocity gradient bias and two-component coincidence are eliminated. The details, including the LDA bias correction, are found in DeGraaff and Eaton (2001). For 5000 samples, the uncertainties for U, $\overline{u'u'}, \overline{v'v'}, \overline{u'v'}$ are estimated as ±1.5%, ±4%, ±8% and ±10% of their local value in the center of the profiles. The average data rate is approximately 25 Hz in the freestream and considerably lower near the wall for the one atmosphere data, 5 Hz in the freestream for the four atmosphere case and 1 Hz in the freestream for the eight atmosphere case. Since the local values of the Reynolds stresses approach zero in the freestream and near the wall, the relative uncertainties in those regions are larger.

The data reported here were acquired under the conditions shown in Table 1. The data were all gathered along the centerline of the wind tunnel in a fixed coordinate system with the x direction along the tunnel and the y direction normal to the flat plate wall. The mean and turbulent stress data taken over the ramp were then rotated by four degrees to make them perpendicular to the wall for the purpose of analysis and scaling. The values for y used in all plots are in the rotated frame and can be taken as perpendicular to the bottom surface of the flow field at all locations.

Table 1
Experimental conditions for three Reynolds number cases

p_{amb} (Pa)	$U_{e,ref}$ (m/s)	$Re_{\theta,ref}$
101,300	20.5	3300
481,000	20.4	14,100
770,000	16.8	20,600

The x-axis locations, x', are the physical locations normalized by the length of the four degree ramp. This non-dimensionalization is used for all locations with the location $x' = 0.00$ being located at the leading edge of the ramp and $x' = 1.00$ representing the trailing edge of the ramp. The upstream flat plate location is therefore located at $x' = -0.33$ using this non-dimensionalization. The reference location is a flat plate boundary layer, where the measured mean and turbulence profiles exhibited typical flat plate behavior for the mean velocity and turbulence (Aubertine and Eaton, 2005).

Wall static pressure data were measured through 0.64 mm diameter surface pressure taps using a Setra differential pressure transducer (model 264). From these wall pressure distributions, the pressure gradient can be calculated along the ramp. This value was then normalized following the work of Clauser (1954), who defined a non-dimensional pressure gradient parameter, $\beta = \frac{\delta^*}{\tau_0}\frac{dP}{dx}$. Here the pressure gradient is normalized using the wall shear stress, τ_0, and the displacement thickness, δ^*. This pressure distribution gives a varying value of β, the Clauser pressure gradient parameter, ranging from 0 on the flat plate, to −1 in the mild favorable pressure gradient before the start of the ramp and to a maximum value of 2.5 along the ramp for the lowest Reynolds number case. The value of β does not remain constant along the length of the ramp, but at all locations it is relatively small, indicating that this is a mild adverse pressure gradient. The maximum value of β observed in this flow is similar to the values from the mild adverse pressure gradient equilibrium boundary layer of Clauser, where the maximum values of β is about 2.3 (Coles and Hirst, 1969). Skåre and Krogstad (1994) found values of β greater than 20 for a flow near separation.

Skin friction measurements were made using the oil-fringe imaging method described by Monson et al. (1993) for all locations except for the two upstream flat plate regions ($x' = -0.33$ and 0.00) in which a log law fit was applied instead. The oil flow is non-intrusive and relates the wall shear to the thinning rate of a line of oil placed on the surface. The oil, Dow Corning 200 fluid, is placed on a surface consisting of 0.13 mm thick green acetate with the back side painted flat black, at several locations and the tunnel is started impulsively. Most of the oil flows downstream during a short transient. The remaining oil forms a thin wedge which when illuminated using green monochromatic light produces interference fringes with a uniform spacing near the leading edge of the oil film. These fringes are imaged using a Kodak high resolution camera (model DC290) when a fringe pattern is evident, typically 10 min. Five independent measurements at each location were performed and the fringe spacing was averaged, with a repeatability of ±2%.

The fringe spacing depends on the skin friction but also on the time history of the flow, the properties of the oil, the surface properties and the viewing angle. Because of these

limitations it is very difficult to estimate the absolute value of the skin friction and instead the ratio of the skin friction at the location of interest to the reference location is used. The time history, oil and surface properties are the same at both locations. For the locations along the ramp, the viewing angle for the measurement and reference locations are different and the relationship between the skin friction, C_f, and fringe spacing, ΔS_f, can be expressed as

$$\frac{C_{f,local}}{C_{f,ref}} = \frac{\Delta S_{f,localimage}}{\Delta S_{f,refimage}} \frac{\cos\left(a\sin\left(\frac{\sin\theta_{light,loc}}{n_{oil}}\right)\right)}{\cos\theta_{camera,loc}} \Bigg/ \frac{\cos\left(a\sin\left(\frac{\sin\theta_{light,ref}}{n_{oil}}\right)\right)}{\cos\theta_{camera,ref}} \quad (1)$$

where n_{oil} is the index of refraction of the oil and the angles can be computed based on the 4° angle of the ramp. The effects of the streamwise pressure gradient on the fringe development can be neglected in this analysis due to the weak pressure gradient over the length of the region in which fringes are located. The overall effects of the streamwise pressure gradient are well captured by the changes along the ramp as described by the previous equation.

3. Results

The overall flow development and a discussion of the changes in the structure of the flow have been described previously in Aubertine and Eaton (2005) for a Reynolds number based on momentum thickness of 3300. The effects due to the changing Reynolds number are described here. In addition, turbulent stress scalings which collapse the data over the range of Reynolds numbers examined here are presented.

Fig. 2 shows the development of the mean flow along the ramp at a momentum thickness based Reynolds number of 3300. The ramp shown in this figure is drawn to scale with the vertical height expanded by a factor of two relative to the horizontal axis to show the near-wall region of the flow more clearly. A constant scale, y/h, is used for the vertical axis to show changes in the location of the peak stress as the flow develops. The flow at $x' = -0.33$ is that of a flat plate boundary layer. At the start of the ramp, the flow accelerates slightly due to the mild favorable pressure gradient caused by the curvature. The boundary layer thickens rapidly in the adverse pressure gradient; δ_{99} increases by approximately 75% along the length of the ramp. There is no inflection point observed in the flow due to the weak adverse pressure gradient. The redevelopment of the mean flow shows that the wake starts to decay, but the flow has not fully recovered to that of a flat plate by the final measurement location.

The development of the streamwise and wall normal stresses are shown in Figs. 3 and 4 respectively at a momentum thickness based Reynolds number of 3300. A fixed quantity measured at the reference location was used to normalize the stresses in order to show the change in the peak stress levels as the flow develops. The DeGraaff and Eaton (2000) flat plate scalings, $u_{\tau,ref}U_{e,ref}$ for the streamwise normal direction and $u^2_{\tau,ref}$ for the wall normal direction were used. The streamwise normal stress development shows that as the flow is subjected to the adverse pressure gradient, an outer plateau develops. This plateau increases in intensity relative to the inner peak as the flow progresses. The inner peak decreases as the skin friction falls. The redevelopment region shows that the plateau starts to decay and the inner peak starts to increase back towards its typical flat plate value downstream of the ramp, but the redevelopment is not complete by the final measurement station. The wall normal stress development shows the peak moving away from the wall and growing in strength as the flow travels along the ramp. In the redevelopment region, the peak starts to decay and spread out.

Table 2 gives the values of some important flow parameters for all three Reynolds number cases along the ramp and for the reference flat plate boundary layer, as well as the symbols used in the following figures to represent the various cases.

The development of the Clauser pressure gradient parameter, β, is shown in Fig. 5 for all three Reynolds numbers plotted against the normalized distance along the test section. The peak value of the parameter β is observed to increase slightly with increasing Reynolds number, but the peak value is still low compared to the

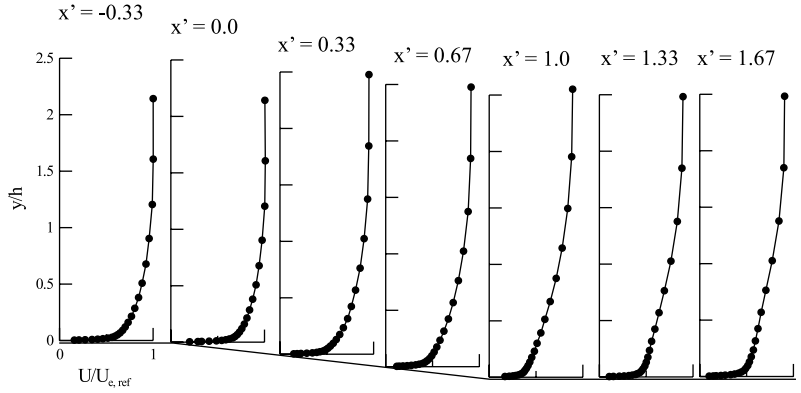

Fig. 2. Mean flow development along the ramp normalized using the fixed quantity, U_e, measured at the reference location, $Re_\theta = 3300$.

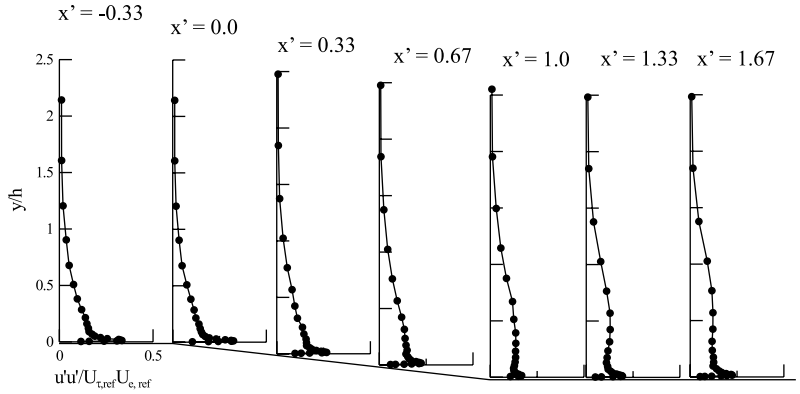

Fig. 3. Streamwise normal stress development along the ramp normalized using the DeGraaff and Eaton scaling, $u_\tau U_e$, measured at the reference location, $Re_\theta = 3300$.

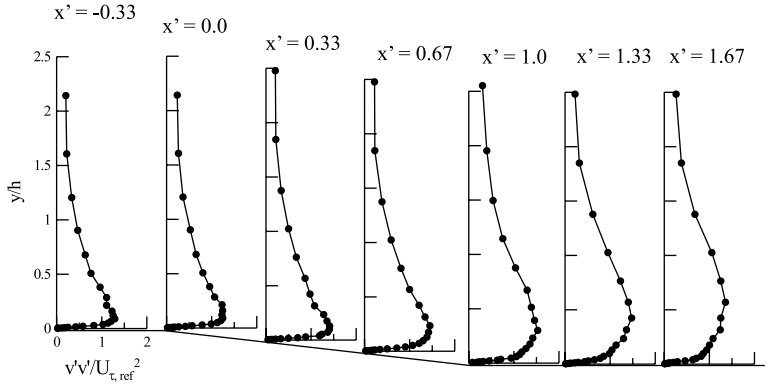

Fig. 4. Wall normal stress development along the ramp normalized using the fixed quantity, u_τ^2, measured at the reference location, $Re_\theta = 3300$.

Table 2
Flow parameters for the three Reynolds numbers and the various measurement locations

Re_θ	x'	U_e (m/s)	δ_{99} (mm)	H	Symbol
3300	−0.33	20.48	25.22	1.34	●
3300	0.25	19.87	29.18	1.39	–
3300	0.5	19.20	33.77	1.42	○
3300	0.75	18.71	37.53	1.48	–
14,100	−0.33	20.39	25.81	1.26	■
14,100	0.25	19.65	31.17	1.31	–
14,100	0.5	18.99	34.57	1.33	□
14,100	0.75	18.50	36.25	1.38	–
20,600	−0.33	16.68	31.57	1.24	♦
20,600	0.25	15.64	35.45	1.29	–
20,600	0.5	15.60	38.87	1.30	◊
20,600	0.75	14.90	39.82	1.38	–

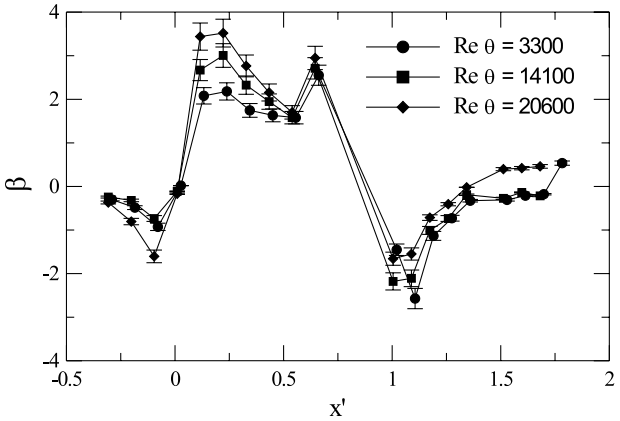

Fig. 5. β development for all three Reynolds numbers, uncertainty as shown.

values of β observed in flows near separation. The effect of Reynolds number variation can be observed to be small with respect to this parameter.

The development of the skin friction coefficient, C_f, is seen in Fig. 6, again plotted against the normalized distance along the test section for all three Reynolds numbers. Increasing the Reynolds number can be seen to decrease the skin friction coefficient on the flat plate. Overall, the trends for all three Reynolds numbers are the same, leading to a decrease of approximately 50% in the value of the skin friction coefficient along the length of the ramp. This is compared to the only 10% decrease in the value of the free-stream velocity over the same distance.

The mean velocity profiles for all three Reynolds numbers are shown in Fig. 7 for the flat plate and the location

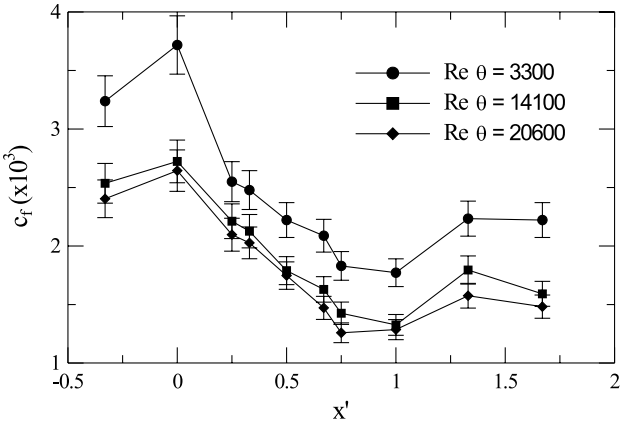

Fig. 6. Skin friction coefficient development for all three Reynolds numbers, uncertainty as shown.

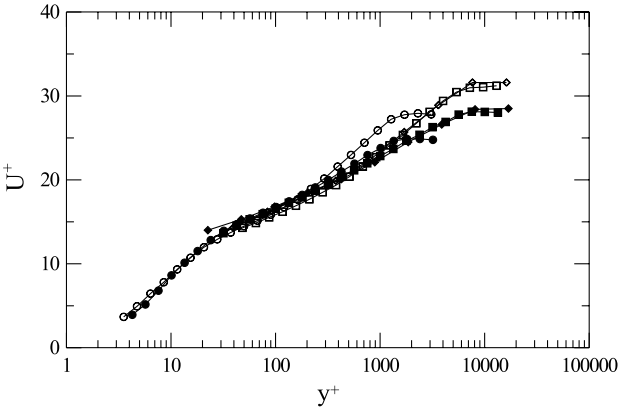

Fig. 7. Mean velocity profiles in inner layer coordinates for the flat plate and halfway down the adverse pressure gradient ramp, solid symbols represent the flat plate location and open symbols represent the adverse pressure gradient location (●) $Re_\theta = 3300$, (■) $Re_\theta = 14{,}100$, (♦) $Re_\theta = 20{,}600$.

halfway down the ramp in inner layer coordinates. The profiles show that the mean velocity profile in the adverse pressure gradient still follows the logarithmic law of the wall, with a growing wake in the outer layer. As the Reynolds number increases, the value of the wake parameter, Π, decreases as expected.

The turbulent normal stress profiles for the flat plate boundary layer and a measurement location halfway down the ramp are shown for all three Reynolds number cases in Figs. 8–11. The streamwise normal stress shows that using the DeGraaff and Eaton (2000) scaling, $u_\tau U_e$ the adverse pressure gradient data collapse in the inner layer, but the peak values do not collapse with those from the flat plate profiles as shown in Fig. 8. In the outer layer the growth of the stress plateau leads to the lack of collapse using these coordinates as seen in Fig. 9. The wall normal stress is shown in Figs. 10 and 11, scaled in the traditional scaling of u_τ^2, which does not collapse the increase in the peak value of the stress in either inner or outer layer coordinates.

For the streamwise normal stress, the DeGraaff and Eaton (2000) flat plate scaling for the inner layer collapses

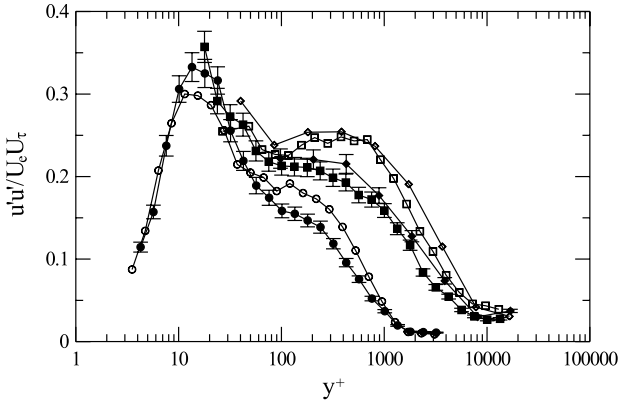

Fig. 8. Inner layer scaling of the streamwise normal stress using the DeGraaff and Eaton flat plate coordinates for the flat plate and halfway down the adverse pressure gradient ramp. Solid symbols represent the flat plate location and open symbols represent the adverse pressure gradient location. (●) $Re_\theta = 3300$, (■) $Re_\theta = 14{,}100$, (♦) $Re_\theta = 20{,}600$. Uncertainty levels shown for flat plate profiles are also indicative of uncertainty for adverse pressure gradient profiles.

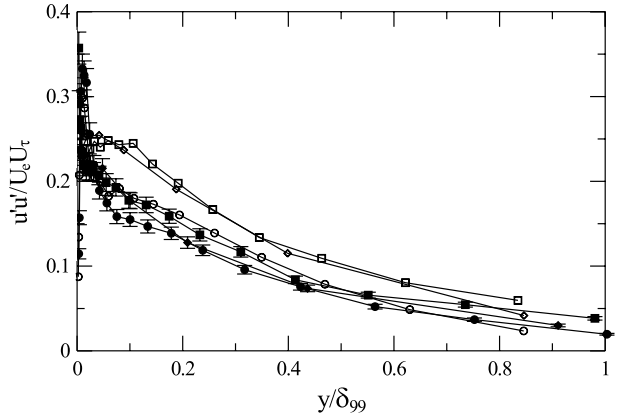

Fig. 9. Outer layer scaling of the streamwise normal stress using the DeGraaff and Eaton flat plate coordinates for the flat plate and halfway down the adverse pressure gradient ramp, symbols as in Fig. 8.

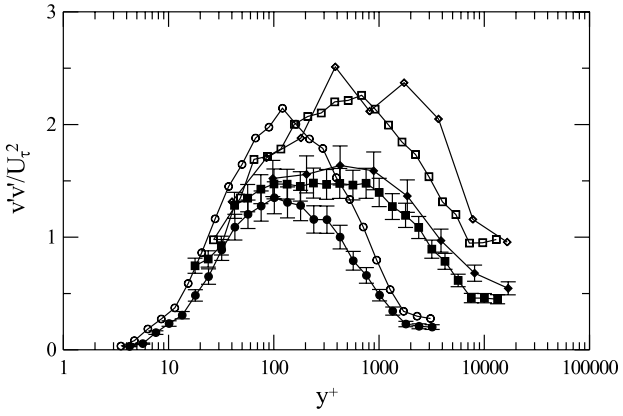

Fig. 10. Inner layer scaling of the wall normal stress using the traditional flat plate coordinates for the flat plate and halfway down the adverse pressure gradient ramp, symbols as in Fig. 8.

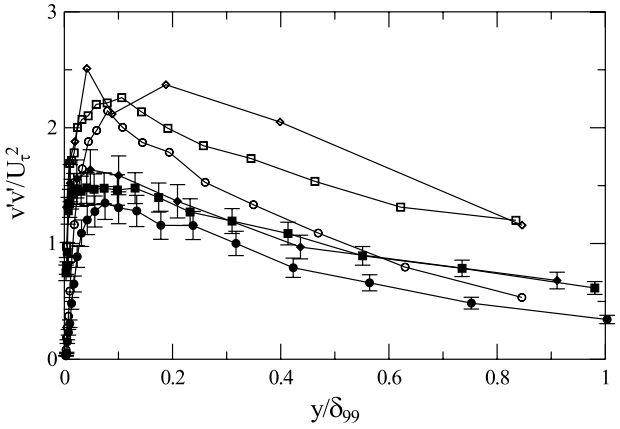

Fig. 11. Outer layer scaling of the wall normal stress using the traditional flat plate coordinates for the flat plate and halfway down the adverse pressure gradient ramp, symbols as in Fig. 8.

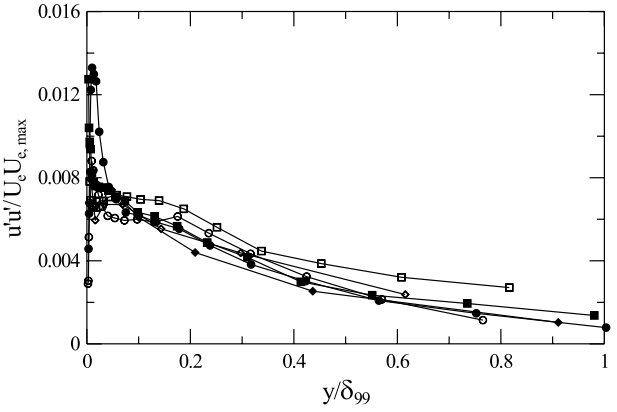

Fig. 13. Streamwise normal stress in outer layer scaling of Elsberry et. al. for the flat plate and three quarters of the way down the adverse pressure gradient ramp, symbols as in Fig. 12.

the adverse pressure gradient profiles along the ramp on each other, but not on the flat plate profile as shown in Aubertine and Eaton (2005). In addition, a plateau develops in the outer layer of the streamwise normal stress profile. The level of the plateau increases as the flow travels along the adverse pressure gradient. This plateau also does not collapse in the scaling of DeGraaff and Eaton (2000). The previously proposed outer layer scaling of Elsberry et al. (2000) was examined for the streamwise normal stress and is shown in Fig. 12 for the flat plate and the location halfway down the ramp. This scaling, in which the stress is normalized by the product of the local freestream velocity and the maximum freestream velocity recorded in the flow field, accounts for the non-equilibrium nature of the outer layer turbulence. Energetic eddies formed upstream continue to produce velocity fluctuations in the decelerating boundary layer. The collapse is far better than that using the flat plate scaling. The Elsberry scaling however does not collapse the inner peak for the adverse pressure gradient data to that of the flat plate profile. In addition, as the flow travels farther down the ramp, the collapse becomes less acceptable as seen in Fig. 13 comparing the flat plate and a location three quarters of the way down the ramp.

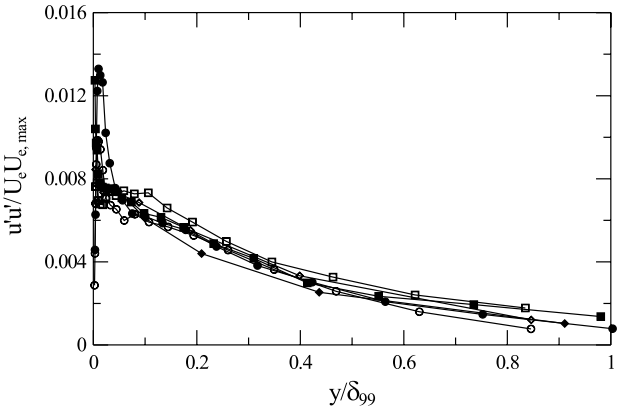

Fig. 12. Streamwise normal stress in outer layer scaling of Elsberry et al. for the flat plate and halfway down the adverse pressure gradient ramp, solid symbols represent the flat plate location and open symbols represent the adverse pressure gradient location, (●) $Re_\theta = 3300$, (■) $Re_\theta = 14{,}100$, (♦) $Re_\theta = 20{,}600$.

The poor inner-layer collapse of the streamwise normal stress shown in Fig. 8 led us to seek an improved scaling that would be applicable to both zero and adverse pressure gradient boundary layers. The success of the DeGraaff and Eaton mixed scaling over a wide range of Reynolds number in zero pressure gradient boundary layers is strong evidence that inner layer streamwise fluctuations are controlled by both inner and outer layer structures. However, the relative strength of the inner and outer contributions changes with Reynolds number and with the pressure gradient. The wake parameter, Π, in some ways reflects the relative velocity jump across the inner and outer regions of the boundary layer. Therefore, mixed scalings that included the wake parameter were explored. Empirically, it was found that normalization of the streamwise stress in the inner layer by $u_\tau^2(1 - 0.5\Pi_{\mathrm{ref}})^2$ provides excellent collapse of the adverse pressure gradient data with the flat plate results. Π_{ref} is the wake function evaluated for the flat plate reference location. This is shown in Fig. 14 for the inner region of the streamwise normal stress, again for the flat plate and a location halfway down the ramp. The data of DeGraaff and Eaton (2000) and Österlund (1999) were also tested with this scaling and good agreement for the inner peak was observed. For the outer layer, a modification to this scaling was determined to collapse the data. The local value of u_τ was replaced with the reference flat plate value, leading to the scaling $u_{\tau,\mathrm{ref}}^2(1 - 0.5\Pi_{\mathrm{ref}})^2$, a constant scaling. This is shown in Fig. 15 for the flat plate and the location halfway down the ramp. The collapse is similar to that observed in the scaling of Elsberry et al. (2000), but appears slightly better as the flow travels further down the ramp. The outer layer streamwise normal stress scaling is based entirely on reference parameters and therefore is a constant scaling indicating that the fluctuations in the outer layer are governed

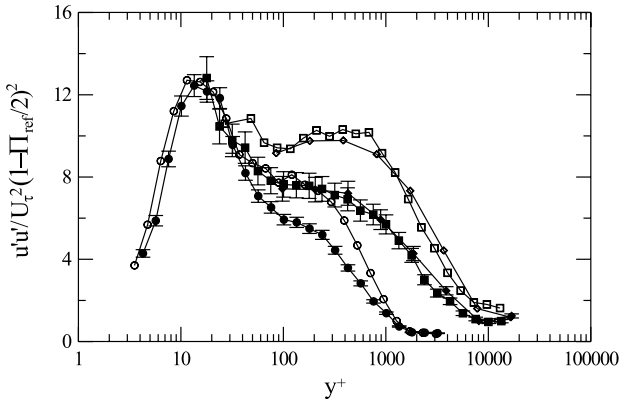

Fig. 14. Streamwise normal stress in new scaling inner layer coordinates for the flat plate and halfway down the adverse pressure gradient ramp, solid symbols represent the flat plate location and open symbols represent the adverse pressure gradient location, (●) $Re_\theta = 3300$, (■) $Re_\theta = 14{,}100$, (♦) $Re_\theta = 20{,}600$ uncertainty levels indicative of all profiles.

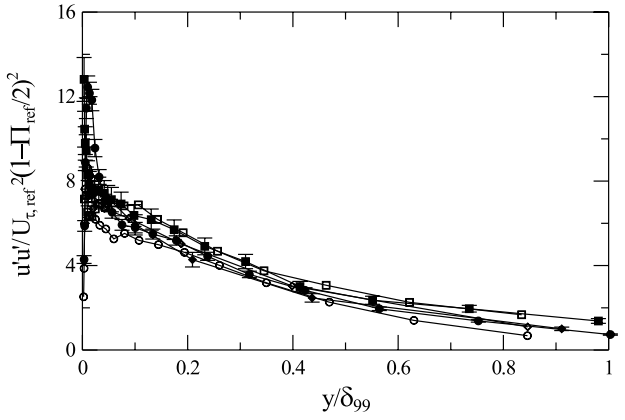

Fig. 15. Streamwise normal stress in new scaling outer layer coordinates for the flat plate and halfway down the adverse pressure gradient ramp, symbols as in Fig. 14.

entirely by the upstream condition. It is only in the near-wall region of the streamwise normal stress that the local conditions of the flow are important to the scaling of the turbulent profiles. To test the applicability of this scaling to other flows, the data of Samuel and Joubert (1974) in an increasingly adverse pressure gradient was used. This is shown in Fig. 16 for the outer layer. The overall collapse is not very good, but this is most likely due to the difficulty in determining the wake parameter, Π_{ref}, for the flow since the first location for which data is available is already subjected to the adverse pressure gradient and therefore no upstream reference location data is available with which to determine the wake function.

The meaning behind the new scaling for the streamwise normal stress was then examined. The constant 0.5 in the scaling was determined empirically by fitting the data measured in this experiment as well as the flat plate data of DeGraaff and Eaton (2000) and Österlund (1999). The wake parameter at the reference location can be determined from the equation

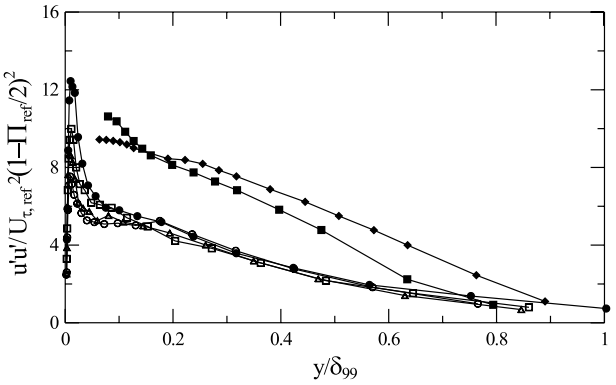

Fig. 16. Streamwise normal stress outer layer scaling including the data of Samuel and Joubert (1974), and the $Re_\theta = 3300$ data from this experiment, symbols as follows (●) $x' = -0.33$, (□) $x' = 0.25$, (△) $x' = 0.50$, (○) $x' = 0.75$, (■) Samuel and Joubert $x = 1.04$ m, (♦) Samuel and Joubert $x = 1.79$ m.

$$\Pi_{\mathrm{ref}} = \frac{\kappa}{2}\left(\frac{2}{\sqrt{C_{\mathrm{f,ref}}}} - B - \frac{1}{\kappa}\ln\left(\frac{\delta_{99}u_{\tau,\mathrm{ref}}}{\nu}\right)\right) \tag{2}$$

Using only the first term in this definition to state that Π is proportional to the inverse of the square root of the skin friction coefficient as described by Elsberry et al. (2000), this can be substituted into the scaling for the inner region for a flat plate boundary layer. This leads to the relationship

$$\frac{\overline{u'u'}}{u_\tau^2\left(1 - \frac{CU_e}{\sqrt{2}u_\tau} + \frac{C^2U_e^2}{8u_\tau^2}\right)} \tag{3}$$

which can be expanded to

$$\frac{\overline{u'u'}}{u_\tau^2 - \frac{CU_eu_\tau}{\sqrt{2}} + \frac{C^2U_e^2}{8}} \tag{4}$$

This scaling is then composed of three components, an inner layer scaling, an outer layer scaling and a mixed scaling and can therefore be considered a more general form of the scaling of DeGraaff and Eaton (2000).

The flat plate wall normal stress scalings shown in Figs. 10 and 11 do not collapse the present data so new scalings were examined. For the wall normal stress, the dimensional values of the peaks in the stress profiles at each Reynolds number were observed to remain approximately constant along the ramp and therefore a constant scaling was expected. To collapse the data over the Reynolds number range examined, the constant scaling chosen was $u_{\tau,\mathrm{ref}}^2$. For the inner layer the scaling is shown in Fig. 17 and the collapse over the range of Reynolds numbers for both the flat plate and the location halfway down the ramp is very good. In addition, the peak value now does not increase with increasing distance down the ramp. The outer region profiles are shown in Fig. 18 where the collapse is

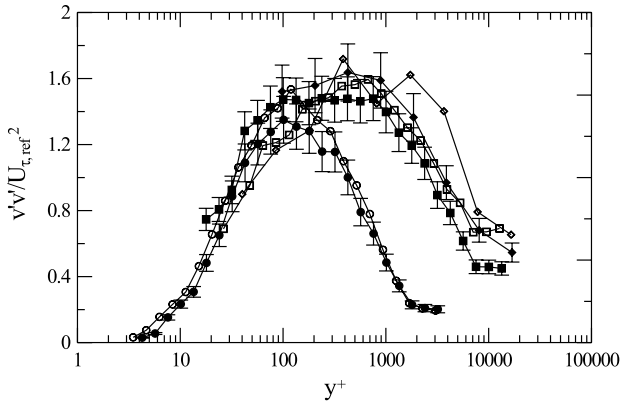

Fig. 17. Wall normal stress in new scaling inner layer coordinates for the flat plate and halfway down the adverse pressure gradient ramp, solid symbols represent the flat plate location and open symbols represent the adverse pressure gradient location, (●) $Re_\theta = 3300$, (■) $Re_\theta = 14{,}100$, (♦) $Re_\theta = 20{,}600$ uncertainty levels indicative of all profiles.

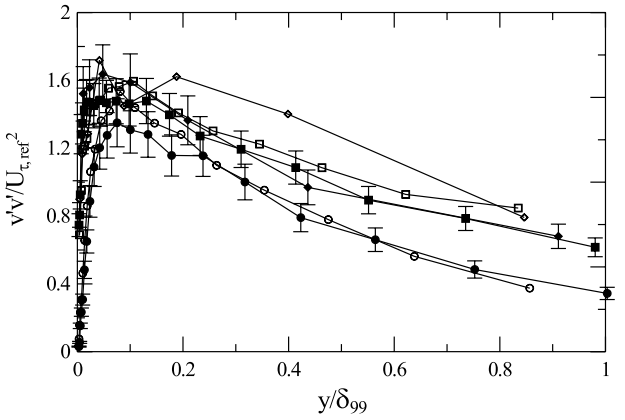

Fig. 18. Wall normal stress in new scaling outer layer coordinates for the flat plate and halfway down the adverse pressure gradient ramp, symbols as in Fig. 17.

observed to be much less acceptable. This is due to the movement of the peak away from the wall as the flow travels down the ramp. Since a simple scaling was the goal of this work, other scalings which may have collapsed these data better were not examined. In addition, no observable Reynolds number trends existed in the data to aid in the collapse. This scaling was then tested using the increasingly adverse pressure gradient data of Samuel and Joubert (1974) and the collapse is shown in Fig. 19. The collapse is quite good in the outer layer. In addition, this scaling agrees with the scaling for the wall normal stress of Song and Eaton (2004) for the flow at the separation point when plotted against the distance from the wall scaled on the inflection point location. The overall interpretation of this scaling is that in a mild adverse pressure gradient, the upstream history of the flow is dominant over the entire boundary layer in the wall normal direction and effect of the adverse pressure gradient is not significant, even up to the point of flow separation if the correct length scale is used.

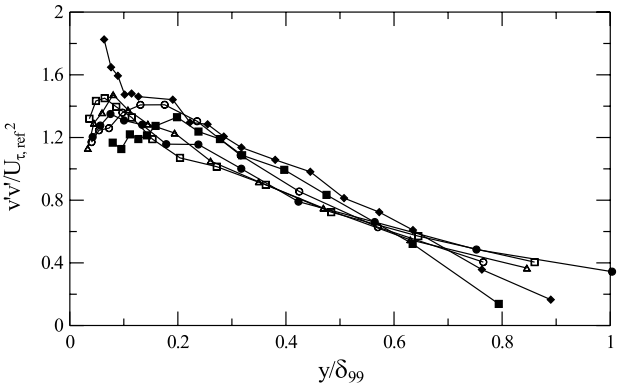

Fig. 19. Wall normal stress outer layer scaling including the data of Samuel and Joubert (1974) and the $Re_\theta = 3300$ data from this experiment, symbols as follows (●) $x' = -0.33$, (□) $x' = 0.25$, (△) $x' = 0.50$, (○) $x' = 0.75$, (■) Samuel and Joubert $x = 1.04$ m, (♦) Samuel and Joubert $x = 1.79$ m.

4. Conclusions

Experimental measurements have been presented for the flow along a four degree expansion ramp in which the Clauser parameter, β, is relatively small and varies slowly. The mean velocity profile in inner coordinates follows the standard logarithmic law of the wall, but the extent of the log region shrinks as the wake occupies a larger fraction of the boundary layer thickness. Although the pressure gradient is mild and there is no inflection point in the mean velocity profile, the boundary layer is not in equilibrium and its shape continues to evolve. The mild adverse pressure gradient causes only small effects on the structure of the turbulence.

Profiles of the two measured Reynolds normal stress components are observed to not collapse using the traditional flat plate scalings in either inner or outer coordinates over the Reynolds number range examined. The streamwise normal stress develops an outer layer plateau that grows as the flow travels down the ramp. The wall normal stress peak increases rapidly as the flow travels along the ramp in the traditional flat plate scaling. New scalings are proposed to collapse the stresses. These scalings show that the wall normal stress in both the inner and outer layer is unaffected by the changing pressure gradient and instead scales using a constant scaling, $u^2_{\tau,\mathrm{ref}}$. The streamwise normal stress in the outer layer is also unaffected by the changing pressure gradient, scaling in a constant scaling while in the inner layer the scaling does depend on the local conditions. The streamwise normal stress scalings, $u^2_\tau(1 - 0.5\Pi_{\mathrm{ref}})^2$ for the inner layer and $u^2_{\tau,\mathrm{ref}}(1 - 0.5\Pi_{\mathrm{ref}})^2$ for the outer layer can be considered more general forms of the mixed scaling of DeGraaff and Eaton (2000) for the flat plate.

5. Description of uncertainty calculations

The uncertainty in the mean velocity and the turbulent stress measurements has been discussed previously, see DeGraaff and Eaton (2001). Propagation of elemental

uncertainties was used to define the overall uncertainties in the non-dimensionalized plots, following the method of Figliola and Beasley (1995).

The uncertainty in the skin friction coefficient was calculated as a function of the statistical uncertainty in the fringe spacing at both the reference and measurement location, the uncertainty in the value of the skin friction at the reference location and the uncertainty in the angle between the camera and light source for the measurements along the ramp. The uncertainty in the value of the reference location skin friction was due to the fit of the flat plate data to the law of the wall and this uncertainty was determined to be 2.5% of the reference value based on the definition

$$\Delta(C_{f,loc})_{C_f} = \frac{\Delta S_{f,loc}}{\Delta S_{f,ref}} \Delta(C_{f,ref}) \tag{5}$$

The uncertainty due to the measurement of the local fringe spacing is given by

$$\Delta(C_{f,loc})_{stat,loc} = \frac{1}{\Delta S_{f,ref}} C_{f,ref} \Delta(\Delta S_{f,loc}) \tag{6}$$

while the uncertainty in the fringe spacing at the reference location is given by

$$\Delta(C_{f,loc})_{stat,ref} = -\frac{1}{(\Delta S_{f,ref})^2} C_{f,ref} \Delta S_{f,loc} \Delta(\Delta S_{f,ref}) \tag{7}$$

These uncertainties are determined from 95% confidence intervals based on the five samples taken at each location and lead to uncertainties of 3.3% and 4.8% of the reference value respectively.

The uncertainty in the angle is calculated in a similar manner and assuming an uncertainty of 2° in θ, the uncertainty is 2.2% of the reference value. Using these values for the uncertainty, the overall uncertainty in the skin friction coefficient can be calculated to be 3.4%. The uncertainty in the friction velocity at any measurement location can then be calculated knowing the freestream velocity.

A similar analysis was performed for the wall static pressure measurements, resulting in the overall uncertainties in the derived pressure gradient parameter β.

Acknowledgement

We gratefully acknowledge the financial support from the Office of Naval Research contract N00014-00-10078.

References

Aubertine, C.D., Eaton, J.K., 2005. Turbulence development in a non-equilibrium turbulent boundary layer with mild adverse pressure gradient. JFM 532, 345–364.

Bernard, A., Foucaut, J.M., Dupont, P., Stanislas, M., 2003. Decelerating boundary layer: a new scaling and mixing length model. AIAA 41 (2), 248–255.

Clauser, F.H., 1954. Turbulent boundary layers in adverse pressure gradients. J. Aero. Sci. 21 (2), 91–108.

Coles, D.E., Hirst, E.A., 1969. In: Proceeding Computation of Turbulent Boundary Layers – 1968 A FOSR-IFP-Stanford Conference, vol. 2, p. 198.

DeGraaff, D.B., Eaton, J.K., 1999. Reynolds number scaling of the turbulent boundary layer on a flat plate and on swept and unswept bumps. Tech Report TSD-118, Stanford University.

DeGraaff, D.B., Eaton, J.K., 2000. Reynolds number scaling of the flat plate turbulent boundary layer. JFM 422, 319–346.

DeGraaff, D.B., Eaton, J.K., 2001. A high resolution laser Doppler anemometer: design, qualification, and uncertainty. Exp. Fluids 20, 522–530.

Elsberry, K., Loeffler, J., Zhou, D., Wygnanski, I., 2000. An experimental study of a boundary layer that is maintained on the verge of separation. JFM 423, 227–261.

Figliola, R., Beasley, D., 1995. Theory and Design of Mechanical Measurements, second ed. John Wiley and Sons.

Klewicki, J., Falco, R., 1990. On accurately measuring statistics associated with small-scale structure in turbulent boundary layers using hot-wire probes. JFM 219, 119–142.

Marusic, I., Kunkel, J.G., 2003. Streamwise turbulence intensity formulation for flat-plate boundary layers. Phys. Fluids 15 (8), 2461–2464.

Mellor, G.L., Gibson, D.M., 1966. Equilibrium turbulent boundary layers. JFM 24, 225–253.

Metzger, M., Klewicki, J., Bradshaw, K., Sadr, R., 2001. Scaling the near-wall axial turbulent stress in the zero pressure gradient boundary layer. Phys. Fluids 13 (6), 1819–1821.

Monson, D.J., Mateer, G.G., Menter, F.R., 1993. Boundary-layer transition and global skin friction measurement with an oil-fringe imaging technique. SAE Tech Paper Series 932550.

Österlund, J., 1999. Experimental studies of zero pressure gradient turbulent boundary layer flow. Ph.D. thesis, Kungl Tekniska Högskolan.

Samuel, A.E., Joubert, P.N., 1974. A boundary layer developing in an increasingly adverse pressure gradient. JFM 66, 481–505.

Skåre, P.E., Krogstad, P.A., 1994. A turbulent equilibrium boundary layer near separation. JFM 272, 319–348.

Skote, M., Henningson, D.S., 2002. Direct numerical simulation of a separated turbulent boundary layer. JFM 471, 107–136.

Song, S., Eaton, J.K., 2004. Reynolds number effects on a turbulent boundary layer with separation, reattachment and recovery. Exp. Fluids 36, 246–258.